Journal of Power Sources 594 (2024) 234005

Contents lists available at ScienceDirect

Journal of Power Sources

journal homepage: www.elsevier.com/locate/jpowsour

Suppressing the self-discharge of high-frequency supercapacitors using electrolytes containing $BaTiO_3$ nanoparticles

Maosheng Wu [a,b], Man Zhao [c,**], Xianmao Lu [a,b,*], Zhong Lin Wang [a,b,d,***]

[a] Beijing Institute of Nanoenergy and Nanosystems, Chinese Academy of Sciences, Beijing, 101400, PR China
[b] School of Nanoscience and Engineering, University of Chinese Academy of Sciences, Beijing, 100049, PR China
[c] State Key Laboratory of Chemical Resources Engineering, College of Chemistry, Beijing University of Chemical Technology, Beijing, 100029, PR China
[d] Yonsei Frontier Lab, Yonsei University, Seoul, 03722, Republic of Korea

HIGHLIGHTS

- Carbonized melamine foams were synthesized for high-frequency supercapacitors (HF–SCs).
- $BaTiO_3$ nanoparticles were employed as electrolyte additive to reduce self-discharge.
- Rate performances and high frequency responses of the HF–SCs were well retained.
- Improved charging efficiency of the HF–SCs by a triboelectric nanogenerator was demonstrated.

GRAPHICAL ABSTRACT

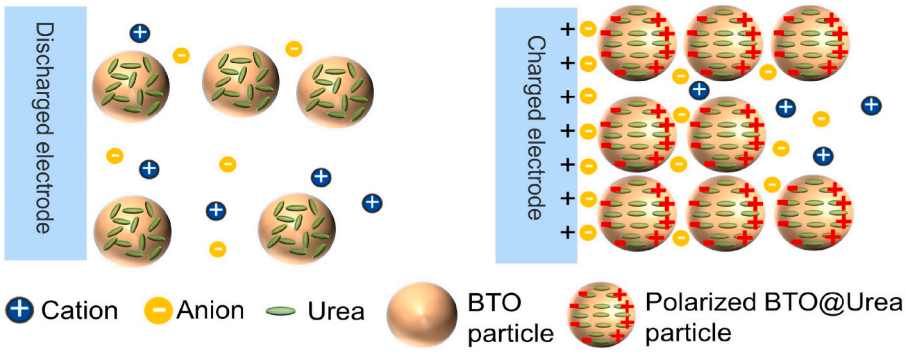

ARTICLE INFO

Keywords:
High-frequency supercapacitors
Self-discharge
$BaTiO_3$ nanoparticles
Triboelectric nanogenerators
Electrorheological effect

ABSTRACT

High-frequency supercapacitors (HF–SCs) are promising electric energy storage devices and alternating current line filters. However, severe self-discharge of HF–SCs causes significant energy loss and limits their applications. Current self-discharge suppression methods for supercapacitors typically lead to decreased rate performance and hence cannot be applied to HF–SCs directly. In this work, barium titanate (BTO) nanoparticles are employed as an electrolyte additive for HF–SCs to reduce self-discharge. By adding BTO nanoparticles into the electrolyte, both leakage current and decay of open circuit voltage of the devices are reduced without sacrificing the specific capacitance and high-frequency response. At a charging voltage of 2 V, the leakage current is reduced by 49 % (3.91 *vs.* 1.98 μA), while the time for the voltage to drop from 2.0 to 1.0 V is extended by 4.5 times (2300 *vs.* 10240 sec). When the HF–SCs with BTO electrolyte are employed to store the energy generated by a triboelectric nanogenerator, the time for charging the cells to 2.0 V is reduced by 82 %. Mechanistic analysis indicates that the reduced self-discharge can be attributed to the fluid electrorheological effect and the enhanced localized electric

* Corresponding author. Beijing Institute of Nanoenergy and Nanosystems, Chinese Academy of Sciences, Beijing, 101400, PR China.
** Corresponding author.
*** Corresponding author. Beijing Institute of Nanoenergy and Nanosystems, Chinese Academy of Sciences, Beijing, 101400, PR China.
E-mail addresses: 2022500073@buct.edu.cn (M. Zhao), luxianmao@binn.cas.cn (X. Lu), zhong.wang@mse.gatech.edu (Z.L. Wang).

https://doi.org/10.1016/j.jpowsour.2023.234005
Received 10 October 2023; Received in revised form 3 December 2023; Accepted 21 December 2023
Available online 30 December 2023

field within the gaps among BTO nanoparticles that lead to sluggish diffusion and migration of reactive species, so the diffusion-controlled faradaic reaction process is suppressed.

1. Introduction

The efficient collection of mechanical energy from ambient environment and conversion into electricity using triboelectric nanogenerators (TENGs) have attracted much attention in recent years [1–5]. However, due to the pulsed nature of the voltage and current outputs of TENGs [6–8], it is often necessary to store the energy generated by TENGs first instead of powering electronic devices directly [9–12]. Supercapacitors (SCs) are promising candidates as energy storge devices for TENGs because of their high charge/discharge rate, wide operating temperature range, and long cycle life [13,14]. The limited frequency responses of typical SCs, however, results in low efficiency when they are used to store high-frequency pulsed energy of TENGs. Recently, various researchers have employed high-frequency supercapacitors (HF–SCs) for TENGs and demonstrated not only the capability of smoothing the pulsed energy as AC line filtering capacitors, but also the benefit of improved energy storage efficiency [15–18]. For examples, Li et al. developed continuous PEDOT:PSS nanomesh films for AC line filtering capacitors with high-frequency responses and integrated with rotating disk TENGs for ripple filtering and pulse energy smoothing [17]. Zhao and coworkers fabricated carbonized melamine foams (CMFs) for HF–SCs to store the energy generated by TENGs and improved the energy utilization efficiency by 20 % compared to typical activated-carbon based SCs [15]. Unfortunately, the self-discharge rates of HF–SCs can be much higher than typical SCs because of the rapid transport of electrolyte ions required for achieving high rate performance [19,20]. Since fast self-discharge causes significant energy loss and compromises the energy storage efficiency, much suppressed self-discharge of HF–SCs has to be achieved for their application in integrating with TENGs to form self-powered systems [15].

In recent years, various strategies targeting at electrode materials, separators, or electrolytes of SCs have been developed to suppress their self-discharge [21,22]. For example, modifications of the electrode materials to reduce the self-discharge rate of SCs have been demonstrated through coating electrodes with a blocking layer, manipulating the functional groups on the electrode surface, or controlling the electrode morphologies [23–27]. Substituting typical separators with polarized membranes to impede the diffusion of electrolyte ions for slow self-discharge has also been reported [28–31]. In addition, different electrolytes, such as bentonite clay@ionic liquid electrolyte, "water--in-salt" electrolytes, polyacrylamide hydrogels, or polyzwitterionic gel electrolytes, have been employed to suppress the self-discharge of SCs [32–39]. Although the above self-discharge suppression methods have proved to be effective for SCs of low-frequency response, they cannot be applied directly to HF–SCs since these methods affect the rate performance and therefore the frequency response adversely.

Previously, we have shown that adding liquid crystal molecules such as 4-*n*-pentyl-4′-cyanobiphenyl into the electrolytes of activated carbon SCs can reduce their self-discharge via the electrorheological (ER) effect which causes increased fluid viscosity and impeded diffusion of ions near the charged electrodes [37,38,40,41]. As a strong dielectric material, $BaTiO_3$ (BTO) nanoparticles dispersed in oil can also lead to the formation of ER fluid since the BTO particles can be polarized into electric dipoles under an applied electric field, changing their original disordered structure into a chain structure [42,43]. When the nanoparticles are coated with a layer of molecules with large dipole moments, the ER effect can be further enhanced and leads to giant electrorheological (GER) effect for further increased viscosity of the fluid [44]. Further more, when the BTO particles are polarized, strong localized electric field in the gaps of the particles can be generated. This localized electric field may also serve as a trap for ionic species and prevent them from fast diffusing [45]. Therefore, we expect that one can take the advantage of both ER and electrostatic confinement effect to suppress the self-discharge of HF–SCs using electrolytes containing BTO nanoparticles.

In this work, we employed BTO nanoparticles coated with urea as an additive to the electrolyte of HF–SCs and demonstrated much reduced self-discharge rate. This was achieved without sacrificing other electrochemical properties such as the specific capacitances and especially the frequency responses of the HF–SCs. Specifically, the leakage current of the HF–SCs was reduced from 3.91 to 1.98 μA after adding 50-nm BTO nanoparticles into the electrolyte. In addition, the time required for 50 % of open circuit voltage (OCV) decay was increased by 4.5 times. More importantly, when the HF–SCs with BTO nanoparticles in the electrolyte was employed to store the energy generated by a TENG, the charging efficiency was improved by 5.6 times. This study demonstrates a new strategy for reducing the self-discharge effectively without compromising the high-frequency responses of HF–SCs.

2. Experimental section

2.1. Preparation of electrode materials

Melamine foams (MFs) were carbonized at high temperature under nitrogen atmosphere using a tube furnace (BTF-1200C, BEQ Equipment Technology, China). The furnace was first warmed up at 400 °C for 30 min before the temperature was raised to 1000 °C at a rate of 2 °C min^{-1}. The MFs were carbonized at 1000 °C for 1 h followed by cooling down to room temperature naturally. The resulting CMFs were cut into circular pieces with a diameter of 8 mm and used as electrodes directly. The mass of each CMF electrode was 0.3 mg.

2.2. Preparation of electrolytes

Preparation of BTO@Urea nanoparticles:First, 1 g of BTO nanoparticles (purchased from Shanghai Puwei Applied Material Technology) were added to 50 mL ethanol and stirred for 1 h. Subsequently, a solution of 0.1 g urea dissolved in ethanol was added to the mixture. After stirring overnight, the suspension was filtered and dried under vacuum to obtain urea-coated BTO particles (denoted as BTO@Urea).

An ionic liquid, 1-ethyl-3-methylimidazolium tetrafluoroborate ($EmimBF_4$, Macklin Reagent Co. Ltd), was used as the electrolyte for the SCs. For BTO-based electrolytes, urea-coated BTO nanoparticles were added to $EmimBF_4$ at a volume ratio of 3:97 under stirring to form a uniform dispersion.

2.3. Materials characterizations

The morphologies of the CMFs and BTO@Urea were examined by a field emission scanning electronic microscope (FESEM, Nova NanoSEM 450) equipped with a Raith/EDAX energy dispersive X-ray spectroscope (EDS). The morphological properties of the BTO nanoparticles were investigated using a high-resolution transmission electron microscope (HR-TEM, FEI Tecnai G2 F20 S-TWIN TMP). Infra-red (IR) spectra were recorded using Fourier transform infrared spectroscopy (FTIR, Bruker Vertex 80 V). The ionic conductivities of the electrolytes were measured by a conductivity meter (Mettler Toledo, Seven Compact S230).

2.4. Electrochemical measurements

A symmetric two-electrode configuration was used for the electrochemical tests of the HF–SCs. CR2032 coin cells were assembled in an

argon-filled glovebox with oxygen and water contents below 0.5 ppm. The volume of the electrolyte was 60 μL. Cyclic voltammetry (CV) scans, galvanostatic charge-discharge (GCD) and electrochemical impedance spectroscopy (EIS) curves were acquired using an electrochemical workstation (CHI660E). EIS was carried out in a frequency range of 1 MHz - 1 Hz at an AC amplitude of 10.0 mV. Self-discharge and leakage currents were obtained using an Arbin BT2000 battery tester system.

The areal capacitances of the electrodes (C_{GCD}) were obtained from GCD curves:

$$C_{GCD} = \frac{2It}{SV} \tag{1}$$

where I is the discharge current of the HF–SCs, t is the discharge time, S is the area of a single electrode, and V is the voltage window.

The specific areal capacitance (C_A) and the imaginary specific areal capacitance (C'') at a frequency (f) were calculated as follows:

$$C_A = -\frac{1}{2\pi f Z'' S} \tag{2}$$

$$C'' = \frac{Z'}{2\pi f |Z|^2 S} \tag{3}$$

where Z', Z'' and $|Z|$ are the real part of the impedance, the imaginary part of the impedance, and the magnitude of the impedance, respectively.

The relaxation time constant (τ_0) was derived from the frequency at the maximum C'' (f_0):

$$\tau_0 = \frac{1}{f_0} \tag{4}$$

For charging test of the SCs by TENG, a rotating TENG (rTENG) was employed (see SI for details of the rTENG). The OCV and short circuit current of the rTENG were recorded by an oscilloscope (Teledyne LeCroy HD 4096) and an electrometer (Keithley 6517), respectively. The rTENG was connected to the HF-SC via a rectifier. The charging curves of the HF–SCs were recorded with the oscilloscope when the rTENG was rotating at 170 rpm.

3. Results and discussion

MFs as highly porous elastic rubber sponges are made of melamine formaldehyde resin via microwave foaming. CMFs, due to their three-dimensional pore structure and nitrogen doping, have been widely used as active electrode materials or support substrates for energy storage and conversion [46]. As shown in Fig. 1a, after carbonization at high temperature, the volume of the MF sponge shrank by nearly 75 %. However, the fibrous three-dimensional pore structure was well retained in the resulting CMFs (Fig. 1b, c and S1a). Elemental analysis via EDS shows that the CMFs contained 90 %, 2 % and 8 % of C, N, and O, respectively (Figs. S1b–e).

Fig. 1d–e are TEM images of the BTO nanoparticles with average diameters of 50 and 100 nm (denoted as BTO50 and BTO100), respectively. The nanoparticles were then coated with urea by mixing the samples with urea solution (denoted as BTO100@Urea, respectively). To verify the presence of urea on the particle surface, FTIR spectra of the samples were obtained. As shown in Fig. 1f, all samples exhibited an absorption peak at 817 cm^{-1}, corresponding to Ti–O stretching vibration [47]. For BTO particles, the peak observed at 3502 cm^{-1} corresponds to the stretching vibration of O–H, while the symmetrical stretching band at approximately 1440 cm^{-1} is attributed to C–O of ester group (-COO) [47]. Following the coating with urea, new absorption peaks emerged at 3345 and 1627 cm^{-1} in the spectra of BTO50@Urea and BTO100@Urea. These absorption peaks are attributed to N–H bond, indicating the presence of urea on the surface of the BTO particles. This observation was further confirmed with SEM-EDS analysis, which shows the presence of N element in the samples after coating with urea (Fig. S2). When the urea-coated BTO nanoparticles were mixed with $EmimBF_4$ ionic liquid, milky electrolytes containing BTO50@Urea or BTO100@Urea were obtained (Fig. S3), indicating good dispersion of the BTO nanoparticles in $EmimBF_4$. Fig. S4 shows the ionic conductivities of the three electrolytes. The $EmimBF_4$ electrolyte without BTO exhibited an ionic conductivity of 15.54 mS cm^{-1}, while slightly decreased ionic conductivities of 15.32 and 14.53 mS cm^{-1} were observed for the electrolytes containing BTO50@Urea and BTO100@Urea, respectively.

HF–SCs were assembled using CMF electrodes with three different electrolytes: $EmimBF_4$ (Blank), $EmimBF_4$ containing 3 vol% of

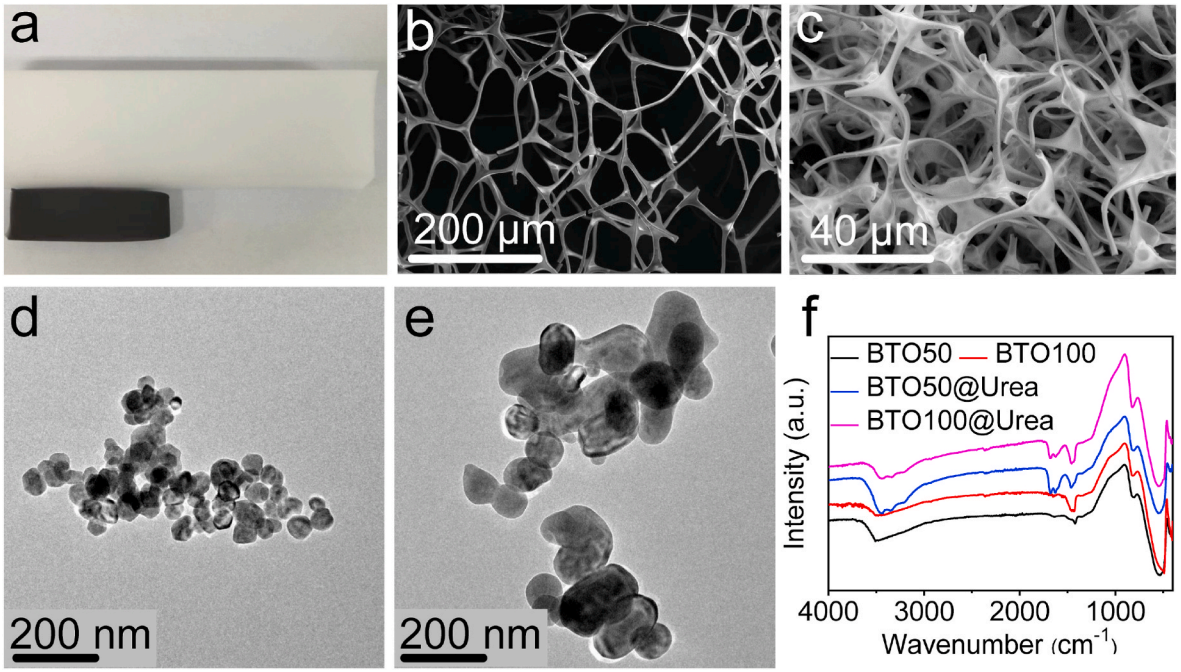

Fig. 1. (a) Digital photos of a piece of MF before and after carbonization at 1000 °C. (b,c) SEM images of the MF (b) before and (c) after carbonization. (d,e) TEM image of (d) BTO50 and (e) BTO100 nanoparticles. (f) FTIR spectra of BTO50 and BTO100 nanoparticles before and after coating with urea.

BTO50@Urea nanoparticles, and $EmimBF_4$ containing 3 vol% of BTO100@Urea nanoparticles, respectively. For all three electrolytes, the CV curves of the HF–SCs exhibited quasi-rectangular shape at scan rates from 10 to 1000 V s^{-1} (Fig. 2a and b), indicating good capacitive behavior of the HF–SCs even at high scan rates. The excellent rate performance of the HF–SCs was also confirmed from the linear increase of discharge current with scan rate (Fig. 2c). The high-frequency responses of the HF–SCs were further examined with EIS. As shown in Fig. 2d, the similar EIS spectra in both low-frequency and high-frequency regions for all three electrolytes indicate that adding BTO nanoparticles into the electrolyte did not affect much on the charge transport properties of the HF–SCs.

Fig. 2e plots the phase angles of the HF–SCs at different frequencies. A phase angle close to −80° at 120 Hz is an important high-frequency performance indicator of SCs [48,49]. For our HF–SCs with Blank, BTO50@Urea, and BTO100@Urea electrolytes, the phase angles at 120 Hz were −74.9°, −74.1°, and −75.7°, respectively, indicating excellent high-frequency responses. The minimum time required to discharge a SC

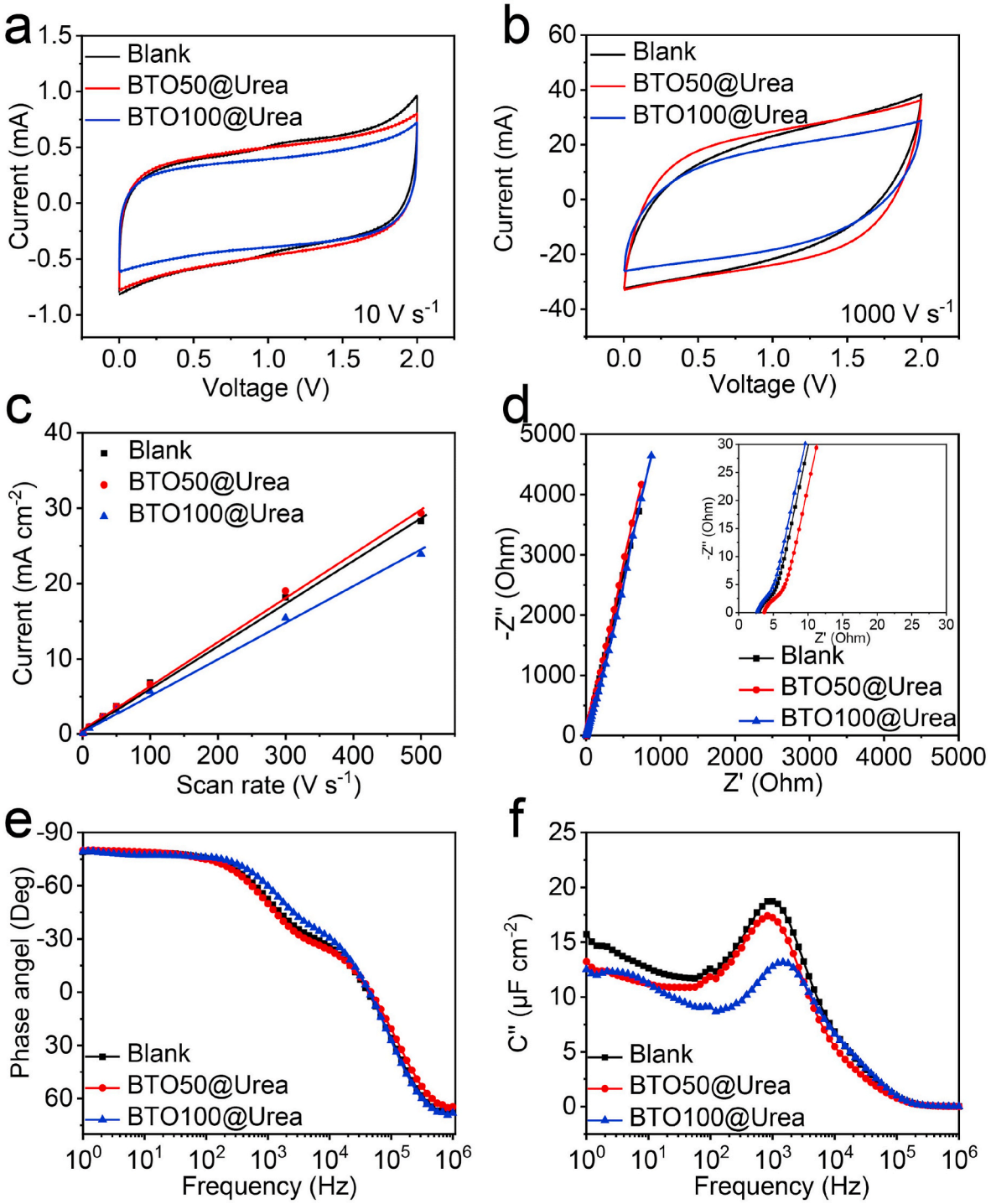

Fig. 2. Electrochemical performances of Blank, BTO50@Urea and BTO100@Urea HF–SCs: (a) CV curves at a scan rate of 10 V s^{-1}, (b) CV curves at a scan rate of 1000 V s^{-1}, (c) plots of discharge current density *vs.* scan rate, (d) Nyquist plots (inset is the enlarged view at high frequencies), (e) phase angles at different frequencies, (f) imaginary part of the specific areal capacitance *vs.* frequency.

with an efficiency larger than 50 %, or relaxation time constant (τ_0), is another important characteristic of HF–SCs. τ_0 can be derived from the reciprocal of frequency at maximum C" (imaginary part of the specific capacitance). Based on the plots of C" *vs.* frequency in Fig. 2f, the τ_0 of the HF–SCs with Blank, BTO50@Urea, and BTO100@Urea electrolytes were 1.06, 1.01 and 0.68 ms, respectively. The small relaxation time constants further confirmed the good high-frequency responses of the HF–SCs. The above results suggest that the high-frequency responses of the HF–SCs were retained after the introduction of urea-coated BTO nanoparticles in $EmimBF_4$ electrolyte.

The GCD curves of the three HF–SCs exhibited quasi-triangular shape at a high current density of 12 mA cm^{-2} (Fig. 3a). The capacitances of the HF–SCs at discharge current densities in the range of 1.2–360 mA cm^{-2} indicate similar rate performances of the HF–SCs, although the one with BTO50@Urea electrolyte was slightly higher than that of Blank and BTO100@Urea (Fig. 3b). At 1.2 mA cm^{-2}, the specific capacitances of the HF–SCs with Blank, BTO50@Urea and BTO100@Urea electrolytes were 201.6, 196.2, and 157.2 μF cm^{-2}, respectively. While the addition of BTO50@Urea nanoparticles into the electrolyte had little effect on the capacitance of the HF-SC, the loss of capacitance for electrolyte with BTO100@Urea nanoparticles may probably be attributed to the larger size of the BTO100 particles which led to smaller exposed surface area of the electrode material. When the current density was increased to 360 mA cm^{-2}, the specific capacitances were 49.0, 56.2 and 46.4 μF cm^{-2} for the HF–SCs with Blank, BTO50@Urea and BTO100@Urea electrolytes, respectively. C_A of the three HF–SCs at different frequencies are plotted in Fig. 3c. At 120 Hz, the specific areal capacitances of the HF–SCs with Blank, BTO50@Urea and BTO100@Urea electrolytes were 49.4, 45.3, and 37.5 μF cm^{-2}, respectively. Cycling stability is another critical parameter for evaluating the performance of HF–SCs. As shown in Fig. 3d, after 100000 cycles of GCD scans at 12 mA cm^{-2}, both HF–SCs with BTO50@Urea and BTO100@Urea nanoparticles showed capacitance retentions higher than that of Blank (97.0 % and 95.0 % *vs.* 91.6 %). Compared to previous studies (Table S1), BTO50@Urea supercapacitor exhibited good electrochemical performances and high-frequency response.

The self-discharge rates of the HF–SCs were first evaluated by leakage currents and OCV decays. To ensure stable performance of the HF–SCs, the devices were cycled between 0 and 2 V for 50 cycles at a current of 20 μA. Afterward, the HF–SCs were charged to 2 V at the same current and held at 2 V for 2 h to minimize the effect of charge redistribution. In the meantime, the float currents required to maintain the voltage of the HF–SCs at 2 V were recorded as the leakage currents. Upon removal of the applied voltage, the OCVs were recorded continuously for 12 h. Fig. 4a shows the leakage currents of the three HF–SCs. For Blank, BTO100@Urea, and BTO50@Urea HF–SCs, the leakage currents at 2 V were 3.91, 2.88, and 1.98 μA, respectively. The reduced leakage currents of BTO100@Urea and BTO50@Urea relative to Blank HF–SCs suggest that the addition of BTO nanoparticles into the electrolyte led to slower self-discharge. The slower self-discharge of HF–SCs with BTO nanoparticles in the electrolyte was also confirmed from OCV decay tests (Fig. 4b). For Blank, BTO50@Urea, and BTO100@Urea

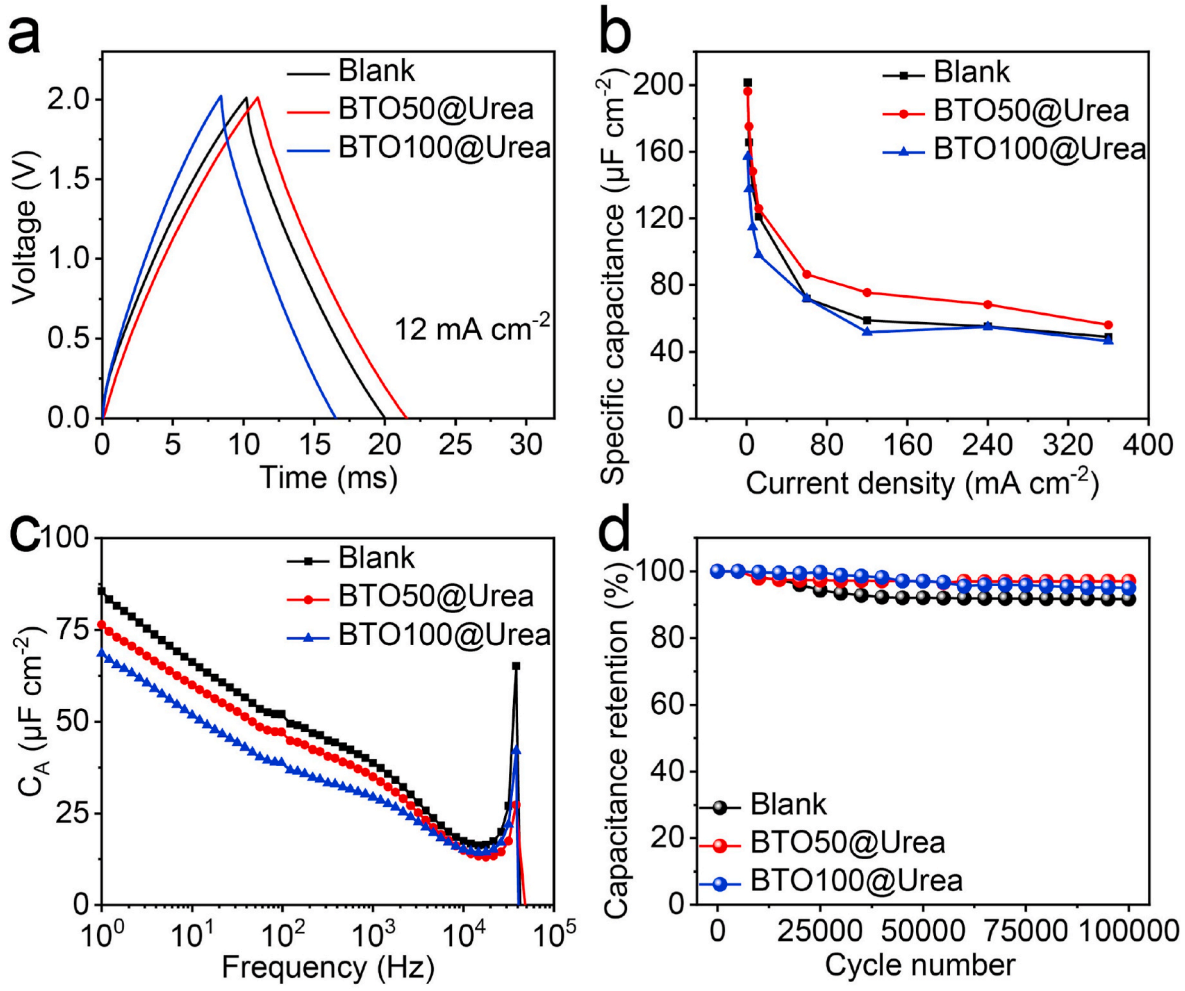

Fig. 3. (a) GCD curves, (b) specific capacitances at different current densities, (c) plots of specific areal capacitance *vs.* frequency, and (d) cycling stability of Blank, BTO50@Urea and BTO100@Urea HF–SCs.

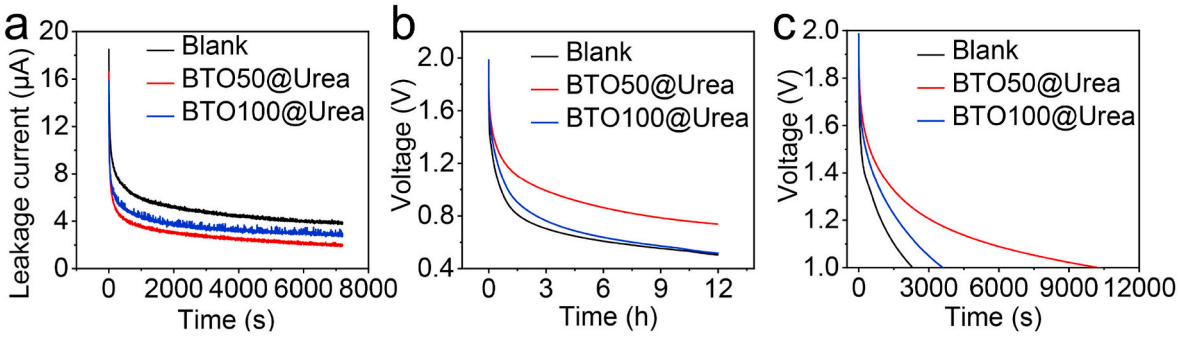

Fig. 4. (a) Leakage currents at 2 V and (b, c) OCV decays of Blank, BTO50@Urea, and BTO100@Urea HF–SCs.

HF–SCs, after 12 h, the OCVs dropped 1.50, 1.27 and 1.49 V, respectively. Clearly, BTO50@Urea exhibited much slower OCV decay than that of Blank and BTO100@Urea HF–SCs. The difference in self-discharge rate of the three HF–SCs was more substantial by examining the time required to reach 50 % of OCV drop – as shown in Fig. 4c, it took 10240, 3600, and 2300 s for BTO50@Urea, BTO100@Urea, and Blank HF–SCs for their OCVs dropped from 2.0 to 1.0 V.

The above results clearly suggest that the addition of BTO@Urea nanoparticles in the electrolyte can significantly reduce the self-discharge rates of the HF–SCs. BTO has a high dielectric constant and can be polarized under external electric field. In the lattice structure of BTO, Ti^{4+} cations occupy the octahedral interstitial sites of [TiO_6]. Because of the high symmetry of the BTO crystal structure, there is no dipole moment without external electric field. Under external electric field, however, Ti^{4+} cations can undergo displacement from the centers of [TiO_6] octahedra, leading to the generation of electric dipoles and polarized electric field on the surface of BTO crystal [50,51]. For the BTO nanoparticles in the electrolyte, when the HF-SC electrodes are discharged, the particles are dispersed randomly (Fig. 5a). After charging, polarization of the BTO particles occurs due to the electric field within the double layer near the electrode surface (Fig. 5b) [52]. In addition, the urea polar molecules affixed to the surface of BTO particles possess the ability not only to facilitate the dispersion of the particles in the electrolyte but also to align themselves in the direction of the electric field, thereby inducing further polarization [42,44,53]. The effect of the polarization of the BTO@Urea particles is twofold. First, it causes alignment of the particles and change in mechanic properties of the surrounding electrolyte such as much-increased fluid viscosity and shear stress attributing to the electrorheological effect [44]. The increased fluid viscosity can lead to impeded diffusion of electrolyte ions and reactive species. Therefore, side reactions via shuttling of the reactive ions and molecules between the positive and negative electrodes are suppressed [52]. Second, when an electric field is applied, the local electric field between two BTO particles increases rapidly as they approach. This localized electrical filed can reach several orders of magnitude higher than the external electric field. For example, Wang et al. found that when an external electric field of 5 kV/cm is applied, the localized electric field between BTO particles can reach approximately 7 MV/cm [54]. The enhanced electric fields among BTO particles added in the electrolyte can act effectively as traps for ionic species and prevent them from diffusing towards the bulk solution and the oppositive electrode. As a result, this synergistic interplay of increased viscosity and electrostatic confinement can lead to significant suppression of diffusion and migration of reactive ions and molecules so that the self-discharge is much reduced. It should be noted that the better performance of BTO50@Urea than that of BTO100@Urea in reducing the self-discharge rate can be attributed to the increased ER effect for particles with smaller size [55].

To elucidate the self-discharge processes of the HF–SCs with electrolytes containing BTO nanoparticles, we further analyzed the voltage decay curves. Based on previous studies [19,20,56–59], the self-discharge of SCs can be divided into three processes: (1) ohmic leakage caused by short circuit between the positive and negative electrodes; (2) charge redistribution due to uneven charging of the electrode materials; and (3) activation-controlled faradaic reaction (ACFR) or diffusion-controlled faradaic reaction (DCFR) processes due to electrode overcharge or the presence of impurities. The self-discharge caused by charge redistribution can be neglected if a sufficient float charging process is applied to the SCs [60,61]. For the self-discharge caused by ohmic leakage and faradaic reaction processes, the following equation can be used to simulate the relationship between the residual voltage (U) and time (t) [37,62]:

$$U = U_0 \exp\left(-\frac{t}{RC}\right) - mt^{\frac{1}{2}} - a - bln\left(t + \frac{CK}{i_0}\right) \quad (5)$$

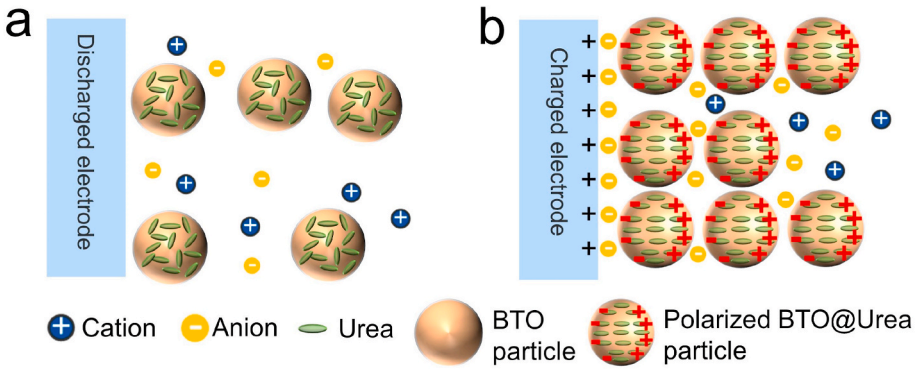

Fig. 5. Schematic illustration of the HF–SCs with BTO nanoparticles in the electrolyte: (a) at discharged state, the ions and BTO nanoparticles in the electrolyte of the HF–SCs are randomly distributed; (b) when the electrodes are charged, the electric field causes polarization of the BTO nanoparticles, leading to enhanced localized electric field within the gaps of the particles as well as electrorheological effect of the surrounding electrolyte.

On the right side of the equation, the first term $U_0 \exp\left(-\frac{t}{RC}\right)$ describes the voltage change of the SC due to ohmic leakage, where U_0 is the initial voltage of the charged SC, R is the leakage resistance, C is the capacitance, and RC corresponds to the time constant of the capacitor. The second term, $-mt^{\frac{1}{2}}$, represents the OCV drop cause by DCFR process, where $m = \frac{2zFAD^{\frac{1}{2}}\pi^{-\frac{1}{2}}C_0}{C}$ is the diffusion coefficient representing the diffusion rate of ions near the electrode surface, z is the amount of charge of the reactive species, D, C_0 and A are the diffusion coefficient, the initial concentration, and the electrode surface area, respectively. The third term, $-a-bln\left(t+\frac{CK}{i_0}\right)$, corresponds to the OCV drop caused by ACFR process, where $a = \frac{R_gT}{\alpha F} ln\frac{\alpha Fi_0}{RTC}$ and $b = \frac{R_gT}{\alpha F}$ are constants related to the faradaic process, α is the charge transfer coefficient, i_0 is the exchange current, T, R_g, F and K are the temperature, ideal gas constant, Faraday constant, and an integral constant, respectively.

Based on the above equation, the self-discharge processes of the HF–SCs were simulated by fitting the measured OCVs with time (Fig. 6a–c). For all three HF–SCs, the OCV changes caused by ohmic leakage were less than 2 mV, indicating that the self-discharge was mainly attributed to ACFR and DCFR processes. For the DCFR process, the diffusion parameter m for Blank HF-SC was estimated to be 4.9 mV s^{-1}, larger than that of BTO100@Urea (1.6 mV s^{-1}) and BTO50@Urea (3.6 mV s^{-1}) HF–SCs. A smaller diffusion parameter indicates smaller transport rate of impurity ions or electrolyte ions, suggesting the addition of BTO nanoparticles in the electrolyte can effectively reduce the self-discharge caused by DCFR process. This was confirmed from the simulated voltage change cause by DCFR: for both BTO50@Urea and BTO100@Urea HF–SCs, slower decays of OCVs attributed to DCFR were revealed compared to Blank HF-SC. The OCV drops after 10000 s caused by DCFR were smaller for BTO50@Urea (0.16 V) and BTO100@Urea (0.36 V) than that of Blank HF-SC (0.49 V) (Fig. 6d). On the other hand, the OCV drops caused by ACFR were similar for all three HF–SCs (0.86, 0.84, and 0.88 V for Blank, BTO50@Urea, and BTO100@Urea, respectively), indicating that adding BTO nanoparticles to the electrolyte did not change much of the ACFR process. This result confirmed that BTO50 nanoparticles reduced the self-discharge of HF–SCs effectively based on the ER effect of the nanoparticles under electric field.

In our previous study, we have shown that HF–SCs can be charged more efficiently by TENGs than commercial activated carbon-based SCs [15]. However, the fast self-discharge of HF–SCs still limits their capability to store the energy generated by TENGs with output currents at μA scale. Developing low self-discharge HF–SCs will benefit the application of self-powered devices charged by TENGs. To demonstrate the advantage of HF–SCs with suppressed self-discharge in storing energy collected by TENGs, the HF–SCs with electrolyte containing BTO nanoparticles were charged by a low-friction rTENG. The charging circuit is shown in Fig. 7a and the structure of the rTENG is illustrated in Fig. 7b (Details of the rTENG can be found elsewhere [63].). Fig. 7c–d shows the rectified voltage and current outputs of the rTENG rotating at 170 rpm. The measured peak OCV and peak short circuit current of the rTENG were 1.4 kV and 18 μA, respectively. The voltage profiles the

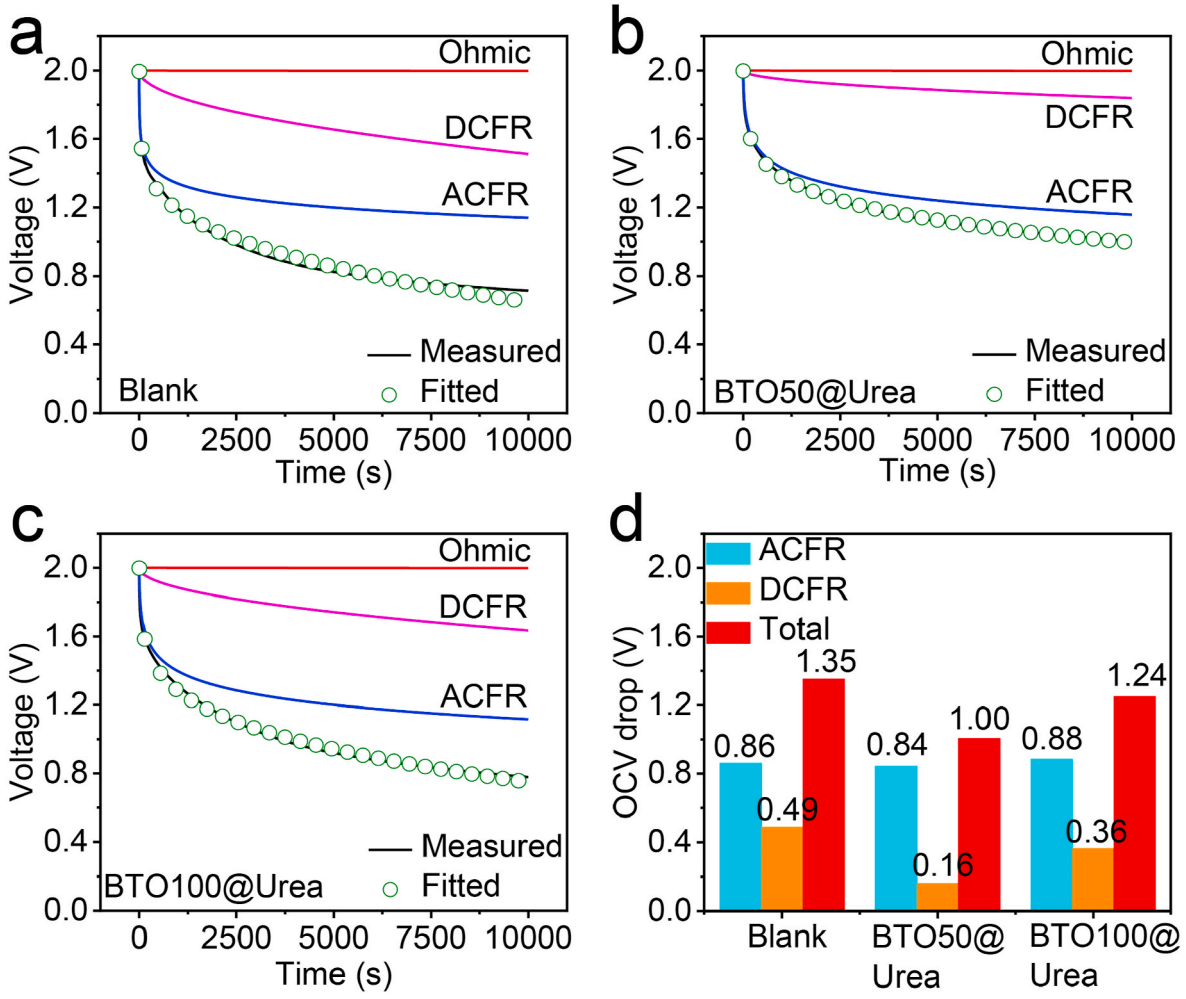

Fig. 6. OCV profiles and fitted curves of (a) Blank, (b) BTO50@Urea, and (c) BTO100@Urea HF–SCs. (d) OCV drops caused by ACFR and DCFR self-discharge processes of the HF–SCs.

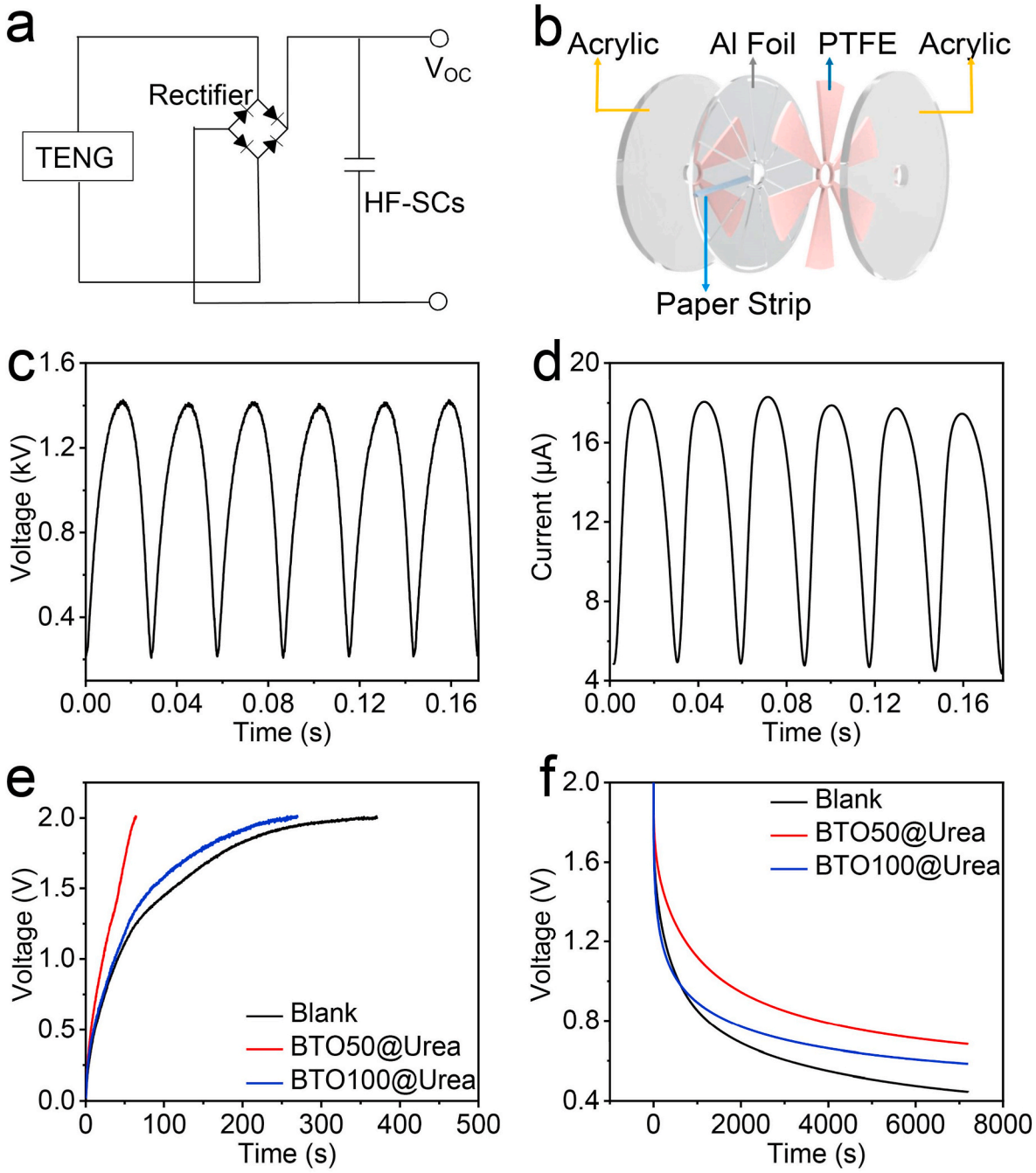

Fig. 7. (a) Circuit for charging HF–SCs by rTENG. (b) Schematic diagram of the rTENG. (c) OCV and (d) short circuit current delivered by the rTENG rotating at 170 rpm. (e) Voltage profiles of the HF–SCs charged by the rTENG. (f) OCV decays of the HF–SCs after charging by the rTENG.

HF–SCs charged by the rTENG are shown Fig. 7e. For Blank, BTO100@Urea, and BTO50@Urea HF–SCs, the times required to charge to 2 V were 370, 270, and 65 s, respectively. The much shorter charging time for BTO50@Urea HF-SC than that of Blank and BTO100@Urea suggests much higher charging efficiency by rTENG. The self-discharge rates of the three HF–SCs after charging by rTENG were also examined. As shown in Fig. 7f, the self-discharge rates of the HF–SCs followed the order of Blank > BTO100@Urea > BTO50@Urea, consistent with the HF–SCs charged by constant currents. The above result demonstrates that the introduction of 50-nm BTO nanoparticles in the electrolyte of the HF–SCs can greatly alleviate their self-discharge and thereby improve the charging rate by rTENG. This much-enhanced energy storage efficiency of HF–SCs make them promising candidates to integrate with TENGs as self-powered systems for collecting micro/nano energy from the ambient environment.

4. Conclusions

In conclusion, we have successfully demonstrated that adding BTO nanoparticles into the electrolytes of HF–SCs can effectively reduce their self-discharge rate without sacrificing other electrochemical performances including specific capacitance and high frequency response. This is because the presence of BTO nanoparticles near the charged electrodes leads to electrorheological effect that causes increased viscosity of electrolyte and impeded diffusion of reactive species. Also, the enhanced localized electric field in the gaps formed among polarized BTO particles can cause electrostatic confinement of ions. Therefore, the self-discharge process attributed to diffusion-controlled faradaic

reactions can be suppressed. As a result, reduced leakage current and OCV decay rates were obtained. When 50-nm BTO nanoparticles coated with urea were introduced into the $EmimBF_4$-based electrolyte of HF–SCs, the leakage current decreased from 3.91 to 1.98 μA and the duration for the OCV to drop from 2.0 to 1.0 V increased from 2300 to 10240 s. Furthermore, we showed that due to the much slower self-discharge rate of the HF–SCs with BTO nanoparticles in the electrolyte, they can be charged from 0 to 2.0 V quickly by a rTENG with a charging efficiency improved by 82 % compared to the HF–SCs without using BTO. This work demonstrates an effective strategy to suppress the self-discharge of HF–SCs while maintaining their high-rate performance.

CRediT authorship contribution statement

Maosheng Wu: Data curation, Formal analysis, Investigation, Methodology, Writing – original draft, Writing – review & editing. **Man Zhao:** Conceptualization, Funding acquisition, Investigation, Methodology, Writing – original draft, Writing – review & editing. **Xianmao Lu:** Conceptualization, Funding acquisition, Investigation, Methodology, Project administration, Supervision, Writing – review & editing. **Zhong Lin Wang:** Conceptualization, Funding acquisition, Supervision, Writing – review & editing.

Declaration of competing interest

The authors declare that they have no known competing financial interests or personal relationships that could have appeared to influence the work reported in this paper.

Data availability

Data will be made available on request.

Acknowledgment

The authors thank the National Natural Science Foundation of China (Fund# 21905026) for the financial support of this work.

Appendix A. Supplementary data

Supplementary data to this article can be found online at https://doi.org/10.1016/j.jpowsour.2023.234005.

References

[1] N. Zhai, Z. Wen, X. Chen, A. Wei, M. Sha, J. Fu, Y. Liu, J. Zhong, X. Sun, Adv. Energy Mater. 10 (2020), 2001041.
[2] S. Niu, Z.L. Wang, Nano Energy 14 (2015) 161–192.
[3] G. Zhu, B. Peng, J. Chen, Q. Jing, Z. Lin Wang, Nano Energy 14 (2015) 126–138.
[4] T. Cheng, Q. Gao, Z.L. Wang, Adv. Mater. Technol. 4 (2019), 1800588.
[5] C. Wu, A.C. Wang, W. Ding, H. Guo, Z.L. Wang, Adv. Energy Mater. 9 (2019), 1802906.
[6] Y. Yu, Z. Li, Y. Wang, S. Gong, X. Wang, Adv. Mater. 27 (2015) 4938–4944.
[7] N. Wang, Y. Liu, E. Ye, Z. Li, D. Wang, Mater. Res. Lett. 10 (2022) 97–123.
[8] Z.L. Wang, Mater. Today 20 (2017) 74–82.
[9] X. Feng, Y. Zhang, L. Kang, L. Wang, C. Duan, K. Yin, J. Pang, K. Wang, Front. Chem. Sci. Eng. 15 (2021) 238–250.
[10] X. Wang, Y. Yang, Nano Energy 32 (2017) 36–41.
[11] S.A. Graham, S.C. Chandrarathna, H. Patnam, P. Manchi, J.-W. Lee, J.S. Yu, Nano Energy 80 (2021), 105547.
[12] Y. Han, W. Wang, J. Zou, Z. Li, X. Cao, S. Xu, Nano Energy 76 (2020), 105008.
[13] Y. Mao, Y. Li, J. Xie, H. Liu, C. Guo, W. Hu, Nano Energy 84 (2021), 105918.
[14] J. Wang, X. Li, Y. Zi, S. Wang, Z. Li, L. Zheng, F. Yi, S. Li, Z.L. Wang, Adv. Mater. 27 (2015) 4830–4836.
[15] M. Zhao, J. Nie, H. Li, M. Xia, M. Liu, Z. Zhang, X. Liang, R. Qi, Z.L. Wang, X. Lu, Nano Energy 55 (2019) 447–453.
[16] W. Li, S. Azam, G. Dai, Z. Fan, Energy Storage Mater. 32 (2020) 30–36.
[17] Z. Li, L. Zhao, X. Zheng, P. Lin, X. Li, R. Li, D. Han, S. Zhao, D. Lv, L. Wang, X. Wang, Y. Zhao, Chem. Eng. J. 430 (2022), 133012.
[18] Z. Li, X. Wang, L. Zhao, F. Chi, C. Gao, Y. Wang, M. Yan, Q. Zhou, M. Zhao, X. Wang, J. Wang, M. Yuan, M. Wu, L. Wang, Y. Zhao, L. Qu, Nat. Commun. 13 (2022) 6359.
[19] M. Zhao, M. Shi, H. Zhou, Z. Zhang, W. Yang, Q. Ma, X. Lu, Electrochim. Acta 390 (2021), 138783.
[20] W. Zhang, W. Yang, H. Zhou, Z. Zhang, M. Zhao, Q. Liu, J. Yang, X. Lu, Electrochim. Acta 357 (2020), 136855.
[21] Y. Wu, R. Holze, Electrochem. Energy Technol. 7 (2021) 1–37.
[22] R. Yuan, Y. Dong, R. Hou, S. Zhang, H. Song, J. Electrochem. Soc. 169 (2022), 030504.
[23] T. Tevi, H. Yaghoubi, J. Wang, A. Takshi, J. Power Sources 241 (2013) 589–596.
[24] Y. Xie, W. Qiao, W. Zhang, G. Sun, L. Ling, N. Carbon Mater. 25 (2010) 248–254.
[25] S. Yuan, X. Huang, H. Wang, L. Xie, J. Cheng, Q. Kong, G. Sun, C. Chen, J. Energy Chem. 51 (2020) 396–404.
[26] Y. Jin, H. Ao, K. Qi, X. Zhang, M. Liu, T. Zhou, S. Wang, G. Xia, Y. Zhu, Mater. Today Energy 19 (2021), 100598.
[27] D. Mishra, N. Kumar, A. Kumar, S.G. Seo, S.H. Jin, J. Mater. Sci. Technol. 113 (2022) 217–228.
[28] C. Zhao, X. Sun, W. Li, M. Shi, K. Ren, X. Lu, ACS Appl. Energy Mater. 4 (2021) 8070–8075.
[29] H. Peng, L. Xiao, K. Sun, G. Ma, G. Wei, Z. Lei, J. Power Sources 435 (2019), 226800.
[30] H. Wang, Q. Zhou, B. Yao, H. Ma, M. Zhang, C. Li, G. Shi, Adv. Mater. Interfac. 5 (2018), 1701547.
[31] W. Yang, Q. Han, W. Li, M. Wu, J. Yao, M. Zhao, X. Lu, Energy Storage Mater. 52 (2022) 29–39.
[32] Z. Wang, X. Chu, Z. Xu, H. Su, C. Yan, F. Liu, B. Gu, H. Huang, D. Xiong, H. Zhang, W. Deng, H. Zhang, W. Yang, J. Mater. Chem. A 7 (2019) 8633–8640.
[33] M. Shi, Z. Zhang, M. Zhao, X. Lu, Z.L. Wang, J. Electrochem. Soc. 168 (2021) 120548.
[34] M. Shi, W. Yang, Z. Zhang, M. Zhao, Z.L. Wang, X. Lu, J. Mater. Chem. A 10 (2022) 2966–2972.
[35] K. Ge, G. Liu, Chem. Commun. 55 (2019) 7167–7170.
[36] J. Chung, H. Park, C. Jung, Electrochim. Acta 369 (2021), 137698.
[37] M. Xia, J. Nie, Z. Zhang, X. Lu, Z.L. Wang, Nano Energy 47 (2018) 43–50.
[38] M. Liu, M. Xia, R. Qi, Q. Ma, M. Zhao, Z. Zhang, X. Lu, Chemelectrochem 6 (2019) 2531–2535.
[39] L. Fan, Q. Tu, C. Geng, J. Huang, Y. Gu, J. Lin, Y. Huang, J. Wu, Electrochim. Acta 331 (2020), 135425.
[40] X. Su, W. Jia, H. Ji, Y. Zhu, J. Energy Storage 41 (2021), 102830.
[41] M. Haque, Q. Li, A.D. Smith, V. Kuzmenko, P. Rudquist, P. Lundgren, P. Enoksson, J. Power Sources 453 (2020), 227897.
[42] L. Li, S. Gao, Mater. Today Commun. 24 (2020), 100993.
[43] W. Jiang, C. Jiang, X. Gong, Z. Zhang, J. Sol. Gel Sci. Technol. 52 (2009) 8–14.
[44] W. Wen, X. Huang, S. Yang, K. Lu, P. Sheng, Nat. Mater. 2 (2003) 727–730.
[45] R. Dubey, A. Mishra, K.N. Singh, P.R. Alapati, R. Dhar, J. Mol. Liq. 225 (2017) 496–501.
[46] Y. Shi, G. Liu, R. Jin, H. Xu, Q. Wang, S. Gao, Carbon Energy 1 (2019) 253–275.
[47] X. Zhang, L. Xu, Q. Wang, J. China Univ. Min. Technol. 17 (2007) 578–581.
[48] K. Sheng, Y. Sun, C. Li, W. Yuan, G. Shi, Sci. Rep. 2 (2012) 247.
[49] N. Islam, J. Warzywoda, Z. Fan, Nano-Micro Lett. 10 (2018) 9.
[50] J.M. Yun, J.H. Shin, J. Ryu, N.M. Shinde, K.H. Kim, Adv. Sustainable Syst. 2 (2018), 1700133.
[51] K. Wu, J. Yi, X. Liu, Y. Sun, J. Cui, Y. Xie, Y. Liu, Y. Xia, J. Zhang, Nano-Micro Lett. 13 (2021) 79.
[52] S. Zhou, X. Meng, C. Fu, D. Xu, J. Li, Q. He, S. Lin, S. Liang, Z. Chang, A. Pan, Small 19 (2023), 2303457.
[53] P. Tan, W.J. Tian, X.F. Wu, J.Y. Huang, L.W. Zhou, J.P. Huang, J. Phys. Chem. B 113 (2009) 9092–9097.
[54] X. Huang, W. Wen, S. Yang, P. Sheng, Int. J. Mod. Phys. B 21 (2007) 4907–4913.
[55] K. Lu, R. Shen, X. Wang, G. Sun, W. Wen, J. Liu, Int. J. Mod. Phys. B 21 (2007) 4798–4805.
[56] S. Subramanian, M.A. Johny, M.M. Neelanchery, S. Ansari, IEEE Trans. Power Electron. 33 (2018) 10410–10418.
[57] H.A. Andreas, J.M. Black, A.A. Oickle, Electrochim. Acta 140 (2014) 116–124.
[58] K. Liu, C. Yu, W. Guo, L. Ni, J. Yu, Y. Xie, Z. Wang, Y. Ren, J. Qiu, J. Energy Chem. 58 (2021) 94–109.
[59] W. Li, W. Yang, M. Wu, M. Zhao, X. Lu, Electrochim. Acta 426 (2022), 140776.
[60] W. Li, M. Wu, W. Yang, M. Zhao, X. Lu, Electrochim. Acta 438 (2023), 141550.
[61] C. Hao, X. Wang, Y. Yin, Z. You, J. Electron. Mater. 45 (2016) 2160–2171.
[62] B.E. Conway, W.G. Pell, T.C. Liu, J. Power Sources 65 (1997) 53–59.
[63] H. Feng, Y. Bai, L. Qiao, Z. Li, E. Wang, S. Chao, X. Qu, Y. Cao, Z. Liu, X. Han, R. Luo, Y. Shan, Z. Li, Small 17 (2021), 2101430.